Malaysian Journal of Chemistry, 2024, Vol. 26(5), 56-62
(Special Issue: *3rd Virtual International Symposium on Sciences 2023*)

Evaluation of Different Metal-Doped ZIF-8 Through Cyclic Voltammetry for Fuel Cell Electrode

Khairul Rijal Razali[1], Muhammad Hafiz Nor Sham[1], Aishah Abdul Jalil[2] and Juan Matmin[1,3]*

[1]Department of Chemistry, Faculty of Science, 81310 Johor Bahru, Johor, Malaysia
[2]Department of Chemical Engineering, Faculty of Energy and Chemical Engineering, 81310 Johor Bahru, Johor, Malaysia
[3]Centre for Sustainable Nanomaterials, Universiti Teknologi Malaysia, 81310 UTM Johor Bahru, Johor, Malaysia
*Corresponding author (e-mail: juanmatmin@utm.my)

This study investigates the impact of various metallic dopants on the structure of zeolitic imidazolate framework (ZIF-8) when used as the anodic electrode in a fuel cell. The wet impregnation method is employed to incorporate different transition metals, including Titanium (Ti), Manganese (Mn), Cobalt (Co), Copper (Cu), Silver (Ag), and Gold (Au), into the ZIF-8 lattice structure. The electrochemical properties of these ZIFs are evaluated using Cyclic Voltammetry (CV) measurements. The CV plots for all electrodes exhibit regular capacitive characteristics, an asymmetric cyclic shape, and oxidation/reduction peaks. The Specific Capacitances (C_P) for period 4 elements follow this increasing order: Cu/ZIF-8 (0.014013568 F/g) < Mn/ZIF-8 (0.017259853 F/g) < Ti/ZIF-8 (0.023771477 F/g) < Co/ZIF-8 (0.097503785 F/g). In the case of group 11 (1B) elements, the CP increases in the following order: Cu/ZIF-8 (0.014013568 F/g) < Ag/ZIF-8 (0.019497694 F/g) < Au/ZIF-8 (0.092614304 F/g). Based on these findings, it is evident that Co/ZIF-8 exhibits superior electrochemical properties for proton conduction and holds promise as a candidate for developing a fuel cell anode.

Keywords: ZIF-8; fuel cell; transition metal dopant; cyclic voltammetry

Received: October 2023; Accepted: February 2024

The expanding population worldwide has driven an increased demand for energy, whether for domestic or industrial purposes. Presently, approximately 80 % of the world's energy demand is met through the supply of fossil fuels [1]. However, these sources are non-renewable and also emit harmful and toxic gases, underscoring the urgent need for a more sustainable energy source [2, 3]. In addition to being renewable and clean, fuel cell offers superior power conversion efficiency, reaching levels as high as 90 %, which surpasses traditional diesel and gas turbine technologies [4-6].

In recent years, traditional metal-based electrodes such as silver, copper, nickel, gold, and titanium have been found to release harmful environmental contaminants and lack durability. To address this issue, researchers are actively developing alternative materials, including conductive polymers, transition metal complexes, and metal-organic frameworks (MOFs) [7-9]. MOFs have gained popularity in fuel cell systems due to their affordability, reliability, and ease of production. They offer high charge density and cost-effectiveness, often demonstrating promising fuel cell properties such as crystallinity, pore size, specific surface area, and low crystal density [10, 11].

However, not all MOFs are suitable as electrode materials due to their unsuitable physical and chemical properties. For example, MOF Material Institute Lavoisier-101 (MIL-101) exhibits low water stability and weak oxidation resistance [12], while CPO-27-Ni has a limited specific surface area and pore volume [13]. On the other hand, ZIF-8, stands out due to its high surface area [14], hierarchical pore structure [15, 16], and excellent thermal stability [14, 17], making it a promising candidate for an MOF-based electrode. Nonetheless, a significant challenge lies in the high charge transfer resistance and large band gap of pristine ZIF-8 [18, 19]. In response, Varangane et al. [20] successfully reduced the band gap by incorporating Cu(II) into its structure, but specific capacitance (C_P) evaluation remains unexplored.

To our knowledge, no prior research has thoroughly assessed various metal-doped ZIF-8 through cyclic voltammetry. This study aims to refine the criteria for selecting transition metals by comparing their performance. Two categories of transition metal precursors, from the fourth period (Ti, Mn, Co, Cu), and group 11 (1B) (Cu, Ag, Au), were incorporated into the ZIF-8 framework. Subsequently, these ZIFs underwent evaluation for their electrochemical properties, including cyclic voltammetry (CV), to assess their suitability as

†Paper presented at the 3rd Virtual International Symposium on Sciences (3rd VISoS 2023)

electrode materials. This research offers valuable scientific insights into the advancement of ZIF-8 materials for achieving heightened energy efficiency in fuel cells, serving as energy conversion devices.

METHODOLOGY

Materials

Zinc nitrate hexahydrate ($Zn(NO_3)_2{\cdot}6H_2O$, Sigma, ≥ 98 %), 2-methylimidazole (2-MeIM, Sigma, ≥ 99 %), triethylamine (TEA, Sigma, ≥ 99.55 %), silver nitrate ($AgNO_3$, Alfa Aesar, ≥ 99 %), titanium isopropoxide (TTIP, Sigma, ≥ 95 %), cobalt (II) nitrate hexahydrate ($Co(NO_3)_2{\cdot}6H_2O$, Sigma, ≥ 98 %), copper (II) nitrate trihydrate ($Cu(NO_3)_2{\cdot}3H_2O$, Sigma, ≥ 98 %), manganese (II) chloride tetrahydrate ($MnCl_2{\cdot}4H_2O$, Sigma, ≥ 99 %), and tetrachloroauric (III) acid trihydrate ($HAuCl_4{\cdot}3H_2O$, Sigma, ≥ 99.5 %) were used in this research.

Preparation of ZIF-8 and Transition Metal/ZIF-8

$Zn(NO_3)_2.6H_2O$, 2-MeIM, and deionized water are mixed in the following ratio of 1:6:500 respectively to create ZIF-8 crystals. The organic linker solution are made by dispersing 2-MeIM (3.312 g) in deionized water (48.45 g), while the metal solution is obtained by completely dissolving $Zn(NO_3)_2.6H_2O$ (2 g) in deionized water (12.11 g). Before combining the metal and ligand solutions, resulting in a cloudy mixture, TEA (3 mL) is gradually introduced into the ligand solution while swirling. The solution was left stirred for 90 min. At this stage of the process, all the precursors for the transition metals were added with varying amount of dopant precursors. The excess reactants are removed from the sediments by washing them three times with deionized water (10 mL x 10 mL x 5 mL) after decanting the residual. The resulting white powder is dried for a minimum of 12 hours at 60℃ in an oven before being ground by using a mortar and then further dried for an additional 12 hours at 120℃.

Characterization

The composition and crystallinity of the samples are confirmed using the X-ray diffraction (XRD, Rigaku) instrument, employing Cu-Kα radiation (λ = 1.54060 Å; 2θ = 0° to 90°). The functional groups are analysed using Fourier transform infrared spectroscopy (FTIR, Perkin Elmer) instrument, covering wavenumbers between 4000 cm^{-1} and 400 cm^{-1}. The specific surface area is calculated using the Brunauer-Emmett-Teller (BET) method.

Electrochemical Measurements

A screen-printed electrode (SPE, DS 110), consisting of the counter electrode, the working electrode (carbon), and the reference electrode (silver), was utilised to conduct tests. Additionally, a potentiostat instrument (Gamry Interphase 1000) was employed to study the electrochemical characteristics of the samples. Prior to testing, 0.01 g of the sample was mixed in a solution of 1 ml deionized water and 10 μl Nafion® 117. After sonication of the mixture for 10 minutes, 20 μL of the supernatant from the sample dispersion was progressively deposited onto SPE. A combination of 0.1 M Na_2SO_4 and 2.5 mM $K_3[Fe(CN)_6]$ was used as the electrolyte in the test (6 ml).

In Cyclic Voltammetry (CV), a voltammogram plot was obtained. The specific capacitance value was then calculated using Equation 1 based on the voltammogram.

$$C_p = \frac{A}{[2mk\ (V_1 - V_2)]} \qquad \text{Equation 1}$$

Where C_p (F/g) represents the specific capacitance, A is the area under the graph, m is the mass of material (0.01 g), k is the scan rate set at 0.0499999 V/s and V_1-V_2 represents the potential window.

RESULT AND DISCUSSION

Chemical Composition

The crystal structure and composition of the samples were analysed using XRD spectroscopy. Figure 1(a) displays the XRD pattern of the ZIF-8 crystal structure. Notably, a strong peak at 7.40° indicates significant crystallinity of ZIF-8 [21]. The XRD patterns reveal sodalite zeolitic crystals for ZIF-8, with diffraction peaks corresponding to the (011), (002), (112), (013), (222), (114), (233), (134), and (044) planes at 7.40°, 10.26°, 12.70°, 16.34°, 18.08°, 21.95°, and 26.52°, respectively. These depicted XRD patterns are remarkably consistent with those described in the literature [14, 22].

Figure 1 shows XRD pattern similar to ZIF-8 for Ti/ZIF-8, Mn/ZIF-8, Co/ZIF-8, Cu/ZIF-8, Ag/ZIF-8, and Au/ZIF-8. It has been clarified that the insertion of different substances into the structure has no effect on ZIF-8's crystallinity, thus maintaining the validity of the MOF [23]. The distinction is evident in the emergence of distinct Ti, Mn, Co, Cu, Ag, and Au peaks in the patterns (see Figure 1). Referring to Figure 1(a), the emergence peak at 36.17°, attributed to (004) plane, can be associated with the presence of Ti. Based on Figure 1(c), the distinctive peaks of the Mn metals were not observed, indicating a possible amorphous phase for the Mn species [24].

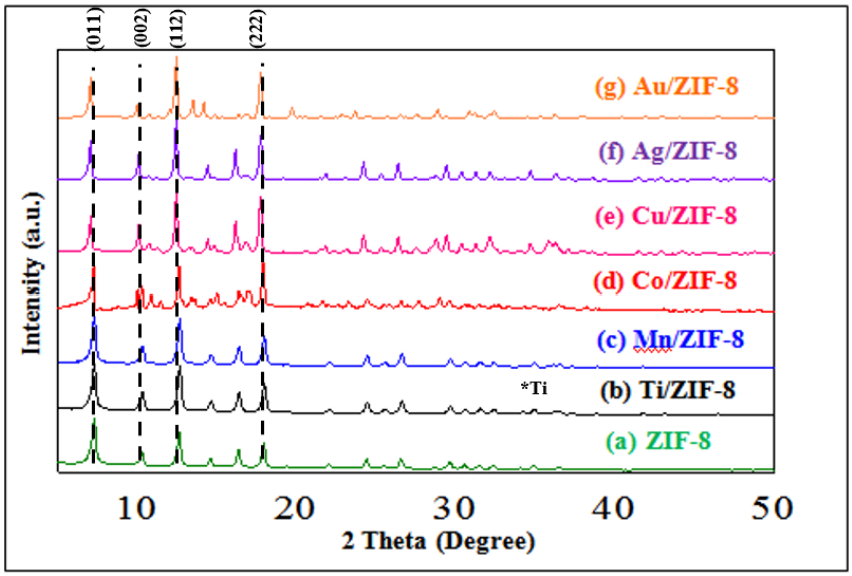

Figure 1. XRD Pattern of (a) ZIF-8, (b) Ti/ZIF-8, (c) Mn/ZIF-8, (d) Co/ZIF-8, (e) Cu/ZIF-8, (f) Ag/ZIF-8 and (g) Au/ZIF-8.

As shown in Figure 1(d), no impurity peaks corresponding to Co species were observed. Interestingly, the intensity of the distinctive diffraction peaks decreased upon the addition of Co particles. Notably, the prominent diffraction peaks expected at 15.1°, 26.5°, and 43.3°, which correspond to the (110), (300), and (315) planes, respectively, were not detected. This observation confirms the successful incorporation of cobalt into both the porous surface and interior of the ZIF-8 structure (see Figure 1(d)).

The functional groups in the samples were analysed using FTIR spectroscopy. Figure 2 displays the FTIR spectra for all samples. The characteristic peaks of ZIF-8 were observed at 1582.50 cm^{-1}, 1423.60 cm^{-1}, 1145.88 cm^{-1}, 995.41 cm^{-1}, and 758.68 cm^{-1}, representing the C=N stretch mode, C-N stretch mode, aromatic C-N stretch mode, C=C stretch mode, and C-H bending mode, respectively. The peaks of the Ti-OH bond at 1337 cm^{-1} confirm the addition of Ti to the frameworks, although they may not be clearly visible due to overlap with other peaks. For Mn/ZIF-8, a peak at 630.47 cm^{-1} is observed, demonstrating the existence of the Mn-N stretching band, consistent with the literature report [24].

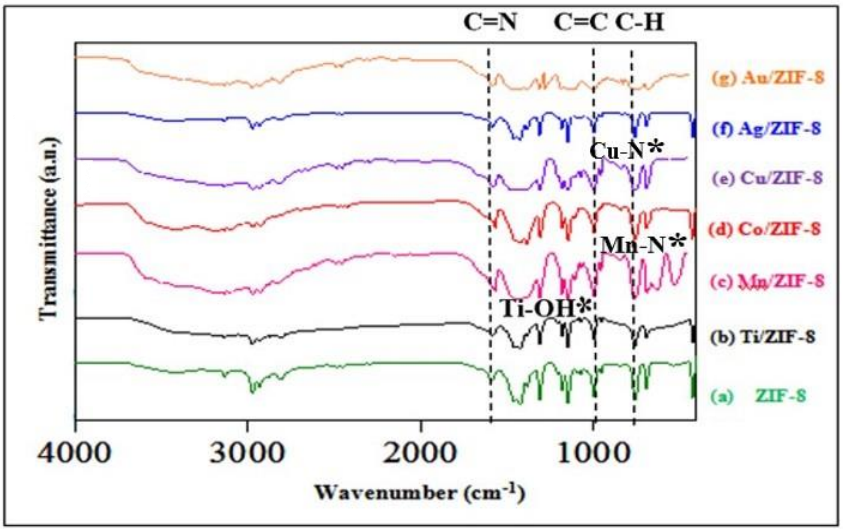

Figure 2. FTIR Spectra of (a) ZIF-8, (b) Ti/ZIF-8, (c) Mn/ZIF-8, (d) Co/ZIF-8, (e) Cu/ZIF-8, (f) Ag/ZIF-8 and (g) Au/ZIF-8.

Table 1. The BET properties of metal doped ZIF samples

Material	Surface Area (m^2/g)	V_{meso} (cm^3/g)	V_{micro} (cm^3/g)	Median Pore Diameter (nm)
ZIF-8	616.49	0.1720	0.1912	61.548
Ag/ZIF-8	375.587	0.0456	0.1383	42.9092
Ti/ZIF-8	143.642	0.0362	0.0985	44.5042
Mn/ZIF-8	303.01	0.0654	0.0922	74.823
Co/ZIF-8	298.692	0.0546	0.0899	43.0163
Cu/ZIF-8	474.11	0.0572	0.1383	28.761
Au/ZIF-8	-	0.0066	0.0029	9.5446

For Co/ZIF-8, it inherits all the base peaks of ZIF-8 along with Zn-N stretching at about 425 cm^{-1}, which is similar to peak reported by Hu et al. [25]. Next, for Cu/ZIF-8, Cu-N bonding vibrations have been identified at 623.68 cm^{-1} within Cu-doped ZIF-8 compounds, consistent with prior studies [26]. Overall, these findings support the notion that the ZIF-8 framework is unaffected by the presence of the dopants.

Surface Area and Pore Size

Figure 3 displays the nitrogen adsorption-desorption results from all the ZIFs. The Brunauer-Emmett-Teller (BET) method was utilised to calculate the specific surface area of ZIF-8, resulting in 616.49 m^2 g^{-1} at relative pressures between 0.00 and 0.15 (Figure 3(a)). The mesopore-size distribution was determined using the Barrett-Joyner-Halenda (BJH) technique by analysing the desorption branches of the isotherms. The median pore diameters are listed in Table 1. The nitrogen isotherm type observed for all ZIFs, as depicted in Figure 3, was found to be Type IV, closely matching previous reports [27, 28].

A hysteresis loop is observed at higher relative pressures, particularly at $P/P_0 > 0.8$ for ZIF-8, due to the presence of large meso/micropores within the ZIF-8 frameworks [29, 30]. This phenomenon was also observed for other ZIFs because the inclusion of the transition metals does not alter the overall frameworks characteristics. Considering the cumulative volume of pores between 1.00 and 400.00 nm in diameter, the mesopore volume (V_{meso}) was calculated to be 0.1720 cm^3 g^{-1}. The micropore volume of ZIF-8 was calculated to be 0.1912 cm^3/g. Table 1 lists the surface area, the V_{meso} and V_{micro} of the doped samples. The results clearly indicate that the doping process negatively impacted the available surface area for active sites. Agglomeration affects the inclination of the isotherms in the low relative pressure range, and the hysteresis loops in the high relative pressure zone serve as indicators of the presence of hierarchical micro-mesopores. The hysteresis loop, H3, which represented the slit-shaped pore, can be observed in all ZIFs as shown in Figure 3.

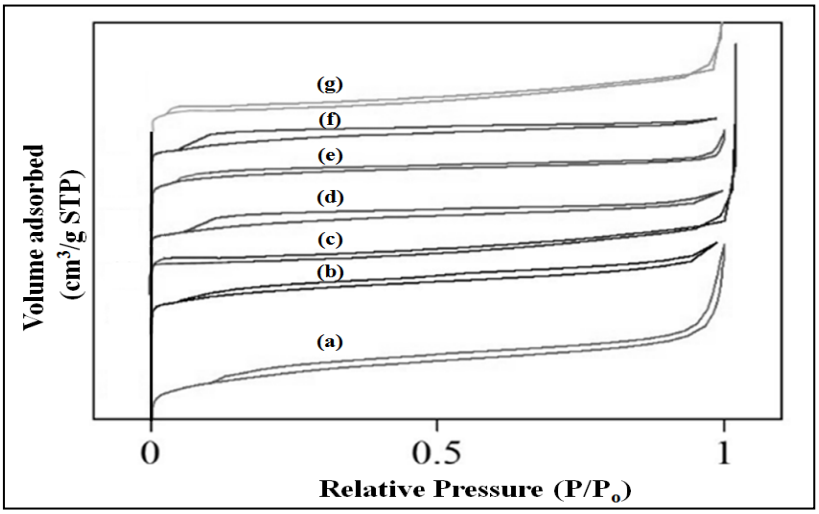

Figure 3. N_2 adsorption-desorption isotherm of (a) ZIF-8, (b) Ti/ZIF-8, (c) Mn/ZIF-8, (d) Co/ZIF-8, (e) Cu/ZIF-8, (f) Ag/ZIF-8 and (g) Au/ZIF-8.

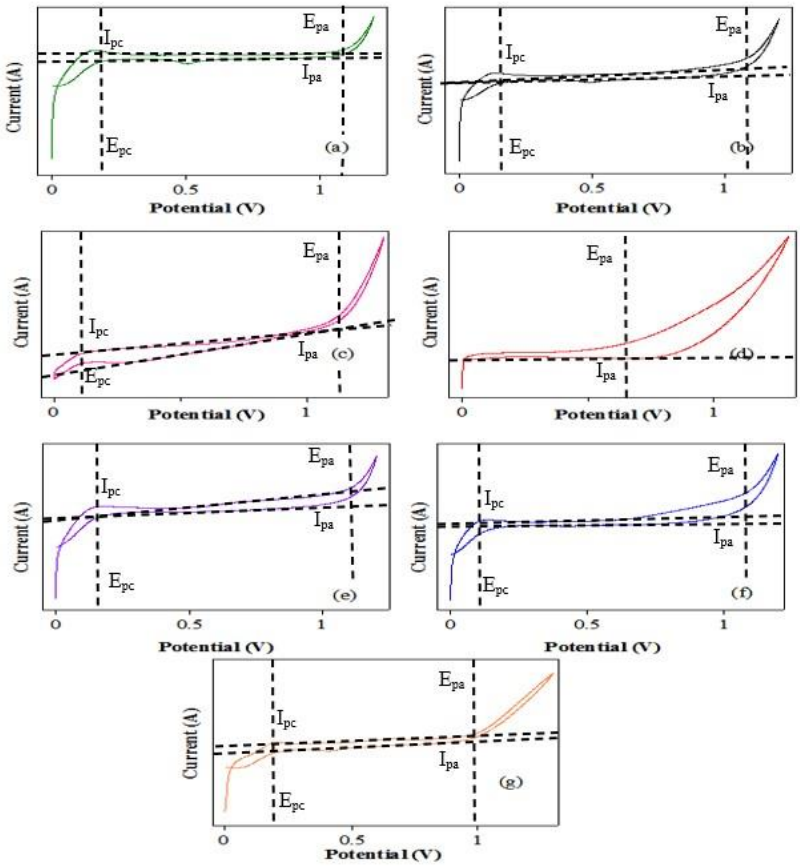

Figure 4. Cyclic voltammograms of (a) ZIF-8, (b) Ti/ZIF-8, (c) Mn/ZIF-8, (d) Co/ZIF-8, (e) Cu/ZIF-8, (f) Ag/ZIF-8 and (g) Au/ZIF-8.

Cyclic Voltammetry

Cyclic voltammetry (CV) is a widely used electrochemical method to investigate the reduction and oxidation of molecular species. Figure 4(a) demonstrates that ZIF-8 exhibits a less pronounced oxidation reaction, as indicated by the more prominent cathodic peak compared to the anodic peak. Except for Co/ZIF-8, the cyclic voltammograms of Ti/ZIF-8, Mn/ZIF-8, Cu/ZIF-8, Ag/ZIF-8, and Au/ZIF-8 share a similar shape to ZIF-8, shown in Figure 4(b), (c), (e), (f), (g), which is known as a quasireversible shape. These species can undergo oxidation and reduction in both directions; however, there are some kinetic barriers that prevent a perfectly reversible reaction. Based on the shape of the voltammograms, it was observed that the cathodic peak current (i_{pc}) is approximately equal to the anodic peak current (i_{pa}), but the peak-to-peak separation (ΔE_P) is significant and not ideal. In contrast, Co/ZIF-8 exhibits an irreversible shape, as depicted in Figure 4 (d), with a prominent anodic peak. This indicates that Co/ZIF-8 can only undergo oxidation and is not reduced back to its original form. Considering that our study aims to identify a material capable of undergoing a high oxidation reaction and serving as the anode in a fuel cell, Co/ZIF-8 is suggested as a potential candidate.

In addition, cyclic voltammetry (CV) is a valuable technique for determining the specific capacity of materials. Therefore, CV measurements were conducted for all ZIFs. The cyclic voltammogram shown in Figure 4 was generated using a voltage range of 0.0–1.2 V and a scan rate of 49.9999 mV/s. Across the entire potential range, from 0.0 to 1.2 V, the CV plots for all electrodes exhibited a regular capacitive characteristic, an asymmetric cyclic shape, and oxidation/reduction peaks. To calculate the specific capacitance (C_p) of the electrodes from the CV curves, Equation 1 was applied. The C_p of the ZIF-8, Ti/ZIF-8, Mn/ZIF-8, Co/ZIF-8, Cu/ZIF-8, Ag/ZIF-8, and Au/ZIF-8, which were found to be 0.015024645 F/g, 0.023771477 F/g, 0.017259853 F/g, 0.097503785 F/g, 0.014013568 F/g, 0.019497694 F/g, and 0.092614304 F/g, respectively.

The value of C_P indicates how large the voltage could be stored when utilising the materials. According to the results, the C_P value is inversely proportional to the R_{ct} values determined by the EIS in the following order: Cu/ZIF-8 < Mn/ZIF-8 < Ti/ZIF-8 < Co/ZIF-8. This is because when the resistance increases, the voltage encountered is expected to increase across the period 4. While going down the group 11 (1B), the C_P followed this

increasing order: Cu/ZIF-8 < Ag/ZIF-8 < Au/ZIF-8, in agreement with the increasing surface area obtained from BET analysis. It is evident that the C_P for the Co/ZIF-8 anode is much greater compared to those for other anode materials. This difference may be due to the electrodes' higher specific surface area along with a larger pore volume.

CONCLUSION

The CV measurements indicated that all ZIFs exhibited oxidation reactions. The C_P for period 4 showed the following increasing order: Cu/ZIF-8 (0.014013568 F/g) < Mn/ZIF-8 (0.017259853 F/g) < Ti/ZIF-8 (0.023771477 F/g) < Co/ZIF-8 (0.097503785 F/g). For group 11 (1B), the C_P followed this increasing order: Cu/ZIF-8 (0.014013568 F/g) < Ag/ZIF-8 (0.019497694 F/g) < Au/ZIF-8 (0.092614304 F/g). Based on these findings, it was observed that Co/ZIF-8 demonstrated superior electrochemical properties for proton passage and could be developed as a fuel cell anode.

ACKNOWLEDGEMENT

The author would like to acknowledge the Ministry of Higher Education (MOHE), Malaysia for financial support via the Fundamental Research Grant Scheme (FRGS) No. FRGS/1/2023/STG04/UTM/02/1 at cost center no.: R.J130000.7854.5F647.

REFERENCES

1. Madadi Avargani, V., Zendehboudi, S., Cata Saady, N. M. and Dusseault, M. B. (2022) A comprehensive review on hydrogen production and utilization in North America: Prospects and challenges. *Energy Conversion and Management*, **269**, 115927.

2. Mufutau Opeyemi, B. (2021) Path to sustainable energy consumption: The possibility of substituting renewable energy for non-renewable energy. *Energy*, **228**, 120519.

3. Hsu, C. J., Atkinson, J. D., Chung, A. & Hsi, H. C. (2021) Gaseous mercury re-emission from wet flue gas desulfurization wastewater aeration basins: A review. *Journal of Hazardous Materials*, **420**, 126546.

4. Singla, M. K., Nijhawan, P., and Oberoi, A. S. (2021) Hydrogen fuel and fuel cell technology for cleaner future: a review. *Environmental Science and Pollution Research*, **28(13)**, 15607–15626.

5. Abdelkareem, M. A., Elsaid, K., Wilberforce, T., Kamil, M., Sayed, E. T. and Olabi, A. (2021) Environmental aspects of fuel cells: A review. *Science of The Total Environment*, **752**, 141803.

6. Haseli, Y. (2018) Maximum conversion efficiency of hydrogen fuel cells. *International Journal of Hydrogen Energy*, **43(18)**, 9015–9021.

7. Symillidis, A., Georgiadou, S. & Lin, W. -F. (2023) Conductive core/shell polymer nanofibres as anode materials for direct ethanol fuel cells. *Advanced Sensor and Energy Materials*, **2(3)**, 100070.

8. Novalin, T., Pan, D., Lindbergh, G., Lagergren, C., Jannasch, P. and Lindström, R. W. (2021) Electrochemical performance of poly(arylene piperidinium) membranes and ionomers in anion exchange membrane fuel cells. *Journal of Power Sources*, **507**, 230287.

9. Abdelkareem, M. A., Wilberforce, T., Elsaid, K., Sayed, E. T., Abdelghani, E. A. M. and Olabi, A. G. (2021) Transition metal carbides and nitrides as oxygen reduction reaction catalyst or catalyst support in proton exchange membrane fuel cells (PEMFCs). *International Journal of Hydrogen Energy*, **46(45)**, 23529–23547.

10. al Obeidli, A., ben Salah, H., al Murisi, M. & Sabouni, R. (2022) Recent advancements in MOFs synthesis and their green applications. *International Journal of Hydrogen Energy*, **47(4)**, 2561–2593.

11. Annapragada, R., Vandavasi, K. R. & Kanuparthy, P. R. (2023) Metal-organic framework membranes for proton exchange membrane fuel cells: A mini-review. *Inorganica Chimica Acta*, **546**, 121304.

12. Steenhaut, T., Hermans, S. and Filinchuk, Y. (2020) Green synthesis of a large series of bimetallic MIL-100 (Fe,M) MOFs. *New Journal of Chemistry*, **44(10)**, 3847–3855.

13. Peralta, D., Barthelet, K., Pérez-Pellitero, J., Chizallet, C., Chaplais, G., Simon-Masseron, A. and Pirngruber, G. D. (2012) Adsorption and separation of xylene isomers: CPO-27-Ni vs HKUST-1 vs NaY. *The Journal of Physical Chemistry C*, **116(41)**, 21844–21855.

14. Ahmad, I., Muhmood, T., Rehman, A., Zahid, M., Abohashrh, M., Nishat, S., Raharjo, Y., Zhou, Z. & Yang, X. (2023) Zeolite imidazole framework entrapped quantum dots (QDs@ZIF-8): encapsulation, properties, and applications. *Journal of the Taiwan Institute of Chemical Engineers*, **149**, 104993.

15. Shahid, S., Baron, G. V., Denayer, J. F. M., Martens, J. A., Wee, L. H. & Vankelecom, I. F. J. (2021) Hierarchical ZIF-8 composite membranes: Enhancing gas separation performance by exploiting molecular dynamics in hierarchical

hybrid materials. *Journal of Membrane Science*, **620**, 118943.

16. Zheng, H., Chen, Y., Yang, J., Hao, P., Ren, L. & Zhou, H. (2023) Bicomponent hydrogels assisted templating synthesis of hierarchically porous ZIF-8 for efficient antibacterial applications. *Journal of Molecular Structure*, **1277**, 134824.

17. Butt, F. S., Lewis, A., Dingwall, F., Mazlan, N. A., Radacsi, N., Fan, X., Chen, X., Yang, Y., Yang, S. & Huang, Y. (2023) ZIF-8 with exceptional thermal stability: Role of organic cosolvents in phase control and structure stabilization. *Materials Today Chemistry*, **34**, 101804.

18. Chang, N., Chen, Y. R., Xie, F., Liu, Y. P. & Wang, H. T. (2021) Facile construction of Z-scheme AgCl/Ag-doped-ZIF-8 heterojunction with narrow band gaps for efficient visible-light photocatalysis. *Colloids and Surfaces A: Physicochemical and Engineering Aspects*, **616**, 126351.

19. Sharma, S. & Chand, P. (2022) Electrochemical behavior of solvothermally grown ZIF-8 as electrode material for supercapacitor applications. *Materials Today: Proceedings*, **76**, 125–131.

20. Varangane, S., Vennapoosa, C. S., Tiwari, A., Nataraj, S. K., Yendrapati, T. P. and Pal, U. (2022) In situ synthesis of Cu-doped ZIF-8 for efficient photocatalytic water splitting. *Applied Organometallic Chemistry*, **36(9)**, e6815.

21. Halim, N. S. A., Wirzal, M. D. H., Bilad, M. R., Nordin, N. A. H. M., Putra, Z. A., Yusoff, A. R. M., Narkkun, T. and Faungnawakij, K. (2019) Electrospun nylon 6,6/ZIF-8 nanofiber membrane for produced water filtration. *Water (Switzerland)*, **11(10)**, 2111.

22. Fazaeli, R. and Aliyan, H. (2019) Novel hierarchical TiO_2@ZIF-8 for photodecolorization of semi-real sample bromothymol blue aqueous solution. *Journal of the Iranian Chemical Society*, **16(1)**, 1–9.

23. Kaur, H., Mohanta, G. C., Gupta, V., Kukkar, D. and Tyagi, S. (2017) Synthesis and characterization of ZIF-8 nanoparticles for controlled release of 6-mercaptopurine drug. *Journal of Drug Delivery Science and Technology*, **41**, 106–112.

24. Farahmand, T., Hashemian, S. and Sheibani, A. (2020) Efficient one-pot synthesis of pyrano[2,3-d]pyrimidinone and pyrido [2,3-d] pyrimidine derivatives by using of Mn-ZIF-8@$ZnTiO_3$ nanocatalyst. *Journal of Molecular Structure*, **1206**, 127667.

25. Hu, L., Yan, Z., Mo, X., Peng, X. & Chen, L. (2020) Hierarchical Co/ZIF-8 as an efficient catalyst for cycloaddition of CO_2 and epoxide. *Microporous and Mesoporous Materials*, **294**, 109917.

26. Chen, X., Yu, Z., Wei, L., Yuan, Z., Sui, X., Wang, Y., Huang, Q., Liao, X. and Chen, Y. (2019) Cobalt nanoparticles confined in carbon cages derived from zeolitic imidazolate frame-works as efficient oxygen electrocatalysts for zinc-air batteries. *Batteries & Supercaps*, **2**, 355–363.

27. Guan, Y., Shi, J., Xia, M., Zhang, J., Pang, Z., Marchetti, A., Wang, X., Cai, J. and Kong, X. (2017) Monodispersed ZIF-8 particles with enhanced performance for CO_2 adsorption and heterogeneous catalysis. *Applied Surface Science*, **423**, 349–353.

28. Sun, W., Zhai, X. and Zhao, L. (2016) Synthesis of ZIF-8 and ZIF-67 nanocrystals with well-controllable size distribution through reverse microemulsions. *Chemical Engineering Journal*, **289**, 59–64.

29. Cravillon, J., Münzer, S., Lohmeier, S. J., Feldhoff, A., Huber, K. and Wiebcke, M. (2009) Rapid room-temperature synthesis and characterization of nanocrystals of a prototypical zeolitic imidazolate framework. *Chemistry of Materials*, **21(8)**, 1410–1412.

30. Lai, Q., Zhao, Y., Liang, Y., He, J. and Chen, J. (2016) In situ confinement pyrolysis transformation of ZIF-8 to nitrogen-enriched meso-microporous carbon frameworks for oxygen reduction. *Advanced Functional Materials*, **26(45)**, 8334–8344.